Mar Biol (2009) 156:355–372
DOI 10.1007/s00227-008-1088-7

ORIGINAL PAPER

# Feeding current characteristics of three morphologically different bivalve suspension feeders, *Crassostrea gigas*, *Mytilus edulis* and *Cerastoderma edule*, in relation to food competition

**Karin Troost · Eize J. Stamhuis · Luca A. van Duren · Wim J. Wolff**

Received: 3 July 2008 / Accepted: 11 November 2008 / Published online: 2 December 2008


**Abstract** Introduced Pacific oysters (*Crassostrea gigas*) have shown rapid expansion in the Oosterschelde estuary, while stocks of native bivalves declined slightly or remained stable. This indicates that they might have an advantage over native bivalve filter feeders. Hence, at the scale of individual bivalves, we studied whether this advantage occurs in optimizing food intake over native bivalves. We investigated feeding current characteristics, in which potential differences may ultimately lead to a differential food intake. We compared feeding currents of the invasive epibenthic non-siphonate Pacific oyster to those of two native bivalve suspension feeders: the epibenthic siphonate blue mussel *Mytilus edulis* and the endobenthic siphonate common cockle *Cerastoderma edule*. Inhalant flow fields were studied empirically using digital particle image velocimetry and particle tracking velocimetry. Exhalant jet speeds were modelled for a range of exhalant-aperture cross-sectional areas as determined in the laboratory and a range of filtration rates derived from literature. Significant differences were found in inhalant and exhalant current velocities and properties of the inhalant flow field (acceleration and distance of influence). At comparable body weight, inhalant current velocities were lower in *C. gigas* than in the other species. Modelled exhalant jets were higher in *C. gigas*, but oriented horizontally instead of vertically as in the other species. Despite these significant differences and apparent morphological differences between the three species, absolute differences in feeding current characteristics were small and are not expected to lead to significant differences in feeding efficiency.

Communicated by S.A. Poulet.

K. Troost · W. J. Wolff
Marine Benthic Ecology and Evolution,
University of Groningen, P.O. Box 14,
9750 AA Haren, The Netherlands

E. J. Stamhuis
Ocean Ecosystems, University of Groningen,
P.O. Box 14, 9750 AA Haren, The Netherlands

K. Troost (✉)
Wageningen IMARES, Yerseke, P.O. Box 77,
4400 AB Yerseke, The Netherlands
e-mail: troost.karin@gmail.com

L. A. van Duren
DELTARES, P.O. Box 177,
2600 MH Delft, The Netherlands

## Introduction

### Introduced oysters

Since their initial introduction in the Oosterschelde estuary (SW Netherlands) in 1964 (Drinkwaard 1999a), Pacific oysters *Crassostrea gigas* (Thunberg) have been spreading rapidly, forming large and dense oyster reefs in the intertidal and subtidal (Drinkwaard 1999b; Wolff and Reise 2002; Dankers et al. 2006). While the Pacific oyster stock in the Oosterschelde estuary was expanding, stocks of the most common native bivalves, the blue mussel *Mytilus edulis* L. and the edible cockle *Cerastoderma edule* (L.) were slightly declining or stable (Geurts van Kessel et al. 2003; Dankers et al. 2006; Troost et al. submitted). This suggests an advantage of *C. gigas* over native bivalve filter feeders. One possible advantage may be found in differences in food intake, caused by a combination of differences in filtration rate and different feeding current characteristics due to differences in morphology.

## Morphology and living habits

In our study area the blue mussel, *M. edulis*, is an epifaunal species living in large beds on hard and soft bottoms both intertidally and subtidally. *M. edulis* circulates water for filtration and respiration through its mantle cavity via in- and exhalant siphons. These siphons are extendible up to a few millimetres. The inhalant siphon is continuous along the entire length of the ventral to posterior edge of the shell and the exhalant siphon is small and conical (Bayne 1976; Gosling 2003). Pacific oysters are epifaunal, and live in beds on hard and soft bottoms both in the intertidal and subtidal. They inhale water through the gape between both mantle folds and the exhalant opening is small relative to the inhalant opening (Gosling 2003). The cockle *C. edule* is an infaunal species living buried in soft sediments both in the intertidal and subtidal. It inhales and exhales water through clearly separated posterior siphons of comparable size that extend several millimetres beyond the margin of the shell (Gosling 2003). When buried the tips of the siphons are usually flush with the sediment, so in the field this species causes very little additional topographic roughness to the sediment surface.

## Feeding currents and food intake

Food intake is for a large part determined by filtration rate, but not entirely. Food intake may for instance be reduced by refiltration of already filtered water. Filtration rates have been extensively studied in many bivalves, including *C. gigas* (Walne 1972; Gerdes 1983; Bougrier et al. 1995; Dupuy et al. 2000), *M. edulis* (Walne 1972; Winter 1973; Foster-Smith 1975; Riisgård 1977; Møhlenberg and Riisgård 1979; Famme et al. 1986; Prins et al. 1996; Smaal and Twisk 1997; Petersen et al. 2004), and *C. edule* (Vahl 1972; Foster-Smith 1975; Møhlenberg and Riisgård 1979; Fernandes et al. 2007; Widdows and Navarro 2007). Filtration rates are in most cases determined by measuring clearance rates of particles that are retained 100% efficiently. Clearance rate is defined as the rate at which a bivalve clears a certain water volume of all suspended particles (Riisgård and Larsen 2000). Clearance rate measurements by different authors have yielded large differences that are related to differences in, e.g. experimental set-up, environmental factors, food quantity and quality, and origin and history of the animals (Riisgård 2001). It is also important to distinguish between results obtained in experiments on actively filtering individuals and experiments on assemblages or even entire shellfish beds. Average clearance rates in a bed will generally be lower than individual clearance rates due to the facts that not all individuals may be active and that within a bed refiltration of previously filtered water can occur. Comparisons between species should therefore ideally be made in the same study. Møhlenberg and Riisgård (1979) compared 13 different species of bivalves, and showed that *C. edule* had higher clearance rates than *M. edulis* at comparable body weight. Walne (1972) compared five species of bivalves and showed that clearance rates of *C. gigas* were more than twice the clearance rates of *M. edulis* at comparable body weight. Based on clearance rates alone, food intake would thus be expected to be higher for *C. gigas* and *C. edule* than for *M. edulis*, at comparable body weight. Since *C. edule* generally has a lower body weight than *M. edulis* and *C. gigas*, and filtration rate is positively related to body weight (Møhlenberg and Riisgård 1978), clearance rates per individual should generally be higher in *C. gigas* than in both *M. edulis* and *C. edule*.

Differences in inhalant feeding current characteristics may also result in differences in food intake. Higher inhalant current velocities will deflect passing larger particles (such as bivalve larvae, see Tamburri et al. 2007) more strongly towards the inhalant aperture, thereby increasing the intake rate of larger food particles. Larger food particles can be larger phytoplankton cells but also zooplankton individuals (Lehane and Davenport 2002; Wong and Levinton 2006; Maar et al. 2007). An ability of adult bivalves to utilize zooplankton as an additional food source may give them an advantage in food competition with species less able to feed on zooplankton (Wong and Levinton 2004). Zooplankton species vary widely in swimming and escape capabilities (Singarajah 1969, 1975; Kiørboe and Visser 1999; Visser 2001). Higher and more strongly accelerating inhalant current velocities are likely to entrain more slow-swimming zooplankton species (Singarajah 1969), although bivalve predation on zooplankton species is also dependent on the sensitivity of the zooplankters to flow-field disturbances and their behavioural reaction to these hydromechanical stimuli (Kiørboe et al. 1999; Titelman and Kiørboe 2003). Inhalant flow fields that extend further into the water column allow for foraging in higher water levels, thereby increasing plankton intake rate (Fréchette et al. 1989).

The supply of phytoplankton and zooplankton to the bivalves is mediated by turbulent mixing of the water column. Turbulent mixing is caused by physical forcing of the system (e.g. tidal forcing). Near-bed turbulence is enhanced by roughness created by biogenic structures (Wright et al. 1997) such as beds of epifaunal bivalves (Butman et al. 1994; Nikora et al. 2002). Turbulence levels are also enhanced by biomixing through the feeding activity of the bivalves. The momentum of exhalant jets increases mixing inside and near the bed, thereby increasing the flux of phytoplankton towards the bivalves (Ertman and Jumars 1988; O'Riordan et al. 1995; Lassen et al. 2006; Van Duren et al. 2006; Fernandes et al. 2007).

Turbulence levels near the bivalve bed may also affect the escape success of zooplankton (Maar et al. 2007). The 'background noise' caused by turbulence may interfere with the perception of the predator (bivalve) signal and thereby enhance the predation risk (Kiørboe et al. 1999). Zooplankton may respond to hydromechanical signals that are present in the inhalant and exhalant flow fields. Exhalant current velocities are generally higher and may present stronger stimuli for escape reactions, but for survival the response to inhalant current should be of more immediate concern.

### Suspension-feeder—flow interactions

Ultimately the effect of the inhalant and exhalant currents on food intake of bivalves is a result of the interaction between the feeding currents and the overlying flow. In turn, the total effect of the presence of bivalves on transport of food from the water column towards the bed is a combination of the interactive effect of their feeding currents with the ambient flow and the interaction of biogenic roughness and ambient flow. For infaunal species such as cockles the latter effect is fairly minor and the filtration activity is important for increasing near-bed mixing and reduction of near-bed depletion (Fernandes et al. 2007). For epibenthic species, such as mussels and Pacific oysters, generally the mixing effect caused by the roughness of the shell aggregations has a more profound effect than the exhalent jets (Wiles et al. 2006), although in some situations, e.g. at low ambient flow conditions, the jets may still have a significant influence (Lassen et al. 2006; Van Duren et al. 2006).

Suspension-feeder—flow interactions in relation to food intake can be studied on different scales: on the scale of the individual, on patch or bed scale, and on estuary scale (Nikora et al. 2002). At these different scales, different processes are relevant. For a complete understanding of how bivalve suspension feeders affect biotic and abiotic parameters and processes and how bivalves are in turn affected by these parameters (Butman et al. 1994; Dame 1996; Wildish and Kristmanson 1997; Nikora et al. 2002; Porter et al. 2004; Van Duren et al. 2006), all scales should ideally be combined. In the present study, we considered one piece of the puzzle: the scale of individual bivalves.

### Aim

Our aim was to study potential differences between feeding current characteristics of individually studied bivalves of three morphologically different species, invasive Pacific oysters *C. gigas* and native mussels *M. edulis* and cockles *C. edule*. These differences may ultimately result in a differential food intake between these species. The study consisted of two parts. First, we empirically studied characteristics of the inhalant flow field. Our null hypothesis was that inhalant feeding current velocities and the acceleration and distance of influence of the inhalant flow field in *M. edulis*, *C. edule* and *C. gigas* are the same (at comparable body weight or shell length). To test this, we analyzed inhalant flow fields in still water using digital particle image velocimetry (DPIV) and particle tracking velocimetry (PTV). Velocity gradients and distances up to which the flow fields influence the surrounding water were determined from the velocity profiles.

Second, we studied whether the three different species of bivalves affect the overlying water column differently with their exhalant jets. With these jets bivalves transfer momentum to the overlying water that may be converted into turbulent kinetic energy. Kinetic energy transfer is a product of the exhalant jet speed and the cross-sectional area of the exhalant aperture (Tritton 1988). Our aim was to explore the order of magnitude of differences in jet speeds between the three bivalve species. Experimental flow quantifying methods such as DPIV and PTV could not be used to study exhalant jet speeds since the bivalves cleared all particles from the water, resulting in an empty exhalant jet. We therefore chose a modelling approach to explore differences in exhalant jet speeds between the three species for a range of exhalant siphon cross-sectional areas and filtration rates. We used dimensions of the exhalant apertures measured by ourselves and filtration rates from literature as input. Implications of differences in exhalant jet speed and exhalant-aperture cross-sectional area for kinetic energy transfer to overlying water layers are discussed.

## Materials and methods

### Experimental animals

Experimental animals were collected from the field. Per species, we collected individuals of different sizes. *C. gigas* were collected by hand from an intertidal oyster bed in the Oosterschelde estuary. Shell lengths ranged from 29 to 174 mm (0.04–1.10 g ash-free dry tissue weight). *M. edulis* were dredged from a subtidal bottom culture plot in the Oosterschelde estuary and ranged in shell length from 11 to 80 mm (0.02–1.21 g). *C. edule* were collected by hand from an intertidal mudflat in the Dutch Wadden Sea. They ranged in shell length from 20 to 32 mm (0.07–0.15 g). All collected animals were transported dry and cooled with ice-packs to the laboratory at Haren as soon as possible, within 24 h. They were left to acclimate for 3 days in an aerated glass aquarium with running seawater of 18°C and 30 psu. The animals were fed with the Instant Algae® Shellfish Diet® (Reed Mariculture Inc., Campbell, CA, USA),

containing *Isochrysis* sp., *Tetraselmis* sp., *Pavlova* sp. and *Thalassiosira weissflogii*. We consulted Helm et al. (2004) and Reed Mariculture (www.reed-mariculture.com) to calculate food rations suitable for growth (2 g dry weight of Shellfish Diet® for every 100 g wet meat weight of bivalves per day).

## Mapping flow fields

Inhalant flow fields of adult cockles, mussels and oysters were mapped using DPIV (e.g. Stamhuis 2006). Per experiment, one animal that was seen to be filtering actively was transferred from the aquarium to a still-water tank (dimensions 40 × 40 × 50 cm), containing filtered seawater that had been well aerated for more than 1 h in advance. All experimental animals were given the same amount of algae (Instant Algae® Shellfish Diet®) upon transfer to the experimental tank, to stimulate feeding. To visualize water movement generated by the bivalve, the water was seeded with neutrally buoyant synthetic white particles (Pliolyte, BASF, diam. 25–50 μm). By transmitting laser light through an optical fibre to a sheet probe, a vertical two-dimensional laser sheet (thickness 0.5 ± 0.2 mm) was projected in the still-water tank. Only particles in this 2D plane were illuminated. We used a CW Krypton laser (Coherent Innova K, Coherent Lasers Inc., Santa Clara, CA, USA; $\lambda = 647$ nm, $P_{max} = 1$ W) for illumination. A high resolution digital camera (Kodak MEGAPLUS ES 1.0, 30 fps at 1,018 × 1,008 px resolution) was mounted perpendicular to the illuminated plane. The camera was linked to a digital acquisition system. For calibration, a piece of plastic centimetre scale was placed in the focal plane next to the experimental animal. After recording a few frames it was removed before the actual experiment started. Analysis of the recorded images was performed with the DPIV software Swift 4.0 (developed at the University of Groningen). Successive filmed frames were analyzed following Stamhuis (2006). We used interrogation areas (sub-images) of 65 × 65 pixels that overlapped by 50%, after image enhancement to remove unevenly lit backgrounds and with increased contrast. Displacement of the particle pattern in the interrogation areas was determined using 'convolution filtering', and the displacement peak was located using the 'centre of gravity weighed to grey value' (Stamhuis 2006 for explanations, details and references). When light-coloured body parts of an animal caused diffusion and reflection of light, thereby possibly disturbing the DPIV analysis close to the animal (Frank et al. 2008), the images to be analyzed were treated in advance by masking the animal itself in Adobe® Photoshop®. Results of the DPIV analyses were exported to Microsoft® Excel© for further analysis.

Because suspension feeders have been reported to reduce their filtration rate in response to high particle loading (e.g. Foster-Smith 1975; Riisgård and Randløv 1981), we kept the seeding density as low as possible, without losing too much resolution in the DPIV analysis. In general, a DPIV interrogation area should contain 8–15 particles (Hinsch 1993). During the experiment, seeding particles had to be replenished regularly because the particles were filtered out by the bivalves. Concentrations of seeding particles ranged approximately between 5 and 15 × $10^3$ per ml.

## Localizing inhalant apertures in oysters

To find the locations of strongest inhalant flow in *C. gigas*, the entire flow field of one oyster (78 mm shell length) was mapped using DPIV. Because shell edges of a Pacific oyster are highly irregular and undulating, it was not possible to map the entire inhalant flow field in one 2D plane. Therefore, multiple 2D maps were recorded, with the laser sheet projected at different locations parallel to the sagittal plane (Fig. 1a). After analyzing image pairs at these different locations, maximum velocity vectors were combined and the area of strongest inhalant current velocities determined. Further recording of inhalant currents of *C. gigas* focused on this area.

## Inhalant feeding currents

Recording of inhalant feeding currents started 1 h after transferring an animal from its tank to the experimental still-water tank, provided with food (Instant Algae® Shellfish Diet®, approximately 2 × $10^4$–4 × $10^4$ cells $ml^{-1}$). White synthetic particles were added as soon as the animal was observed to be feeding in its new environment. In order to determine maximum velocities at the inhalant apertures of the bivalves, the laser sheet was projected to cross-sect the plane between valves (the sagittal plane) at a location along the shell edge of interest for *C. gigas* and *M. edulis* and cross-secting the inhalant siphon in *C. edule* (Fig. 2a–c). Cockles were placed upright in black grit, buried halfway. In a natural situation they would also be oriented upright, but buried completely. Mussels were placed upright, with the anterior end of the shell stuck loosely in a rubber ring that was buried in the grit (Fig. 2b). Valve movement was unobstructed by this ring. The experimental position of the mussels roughly corresponded to the orientation of mussels in natural mussel beds with high densities. Mussels generally attach with their ventral surface to the substrate, or to each other in more crowded circumstances when they show a preference for an upright position with the anterior end pointed downward (Maas Geesteranus 1942). Small oysters (78–82 mm) were placed

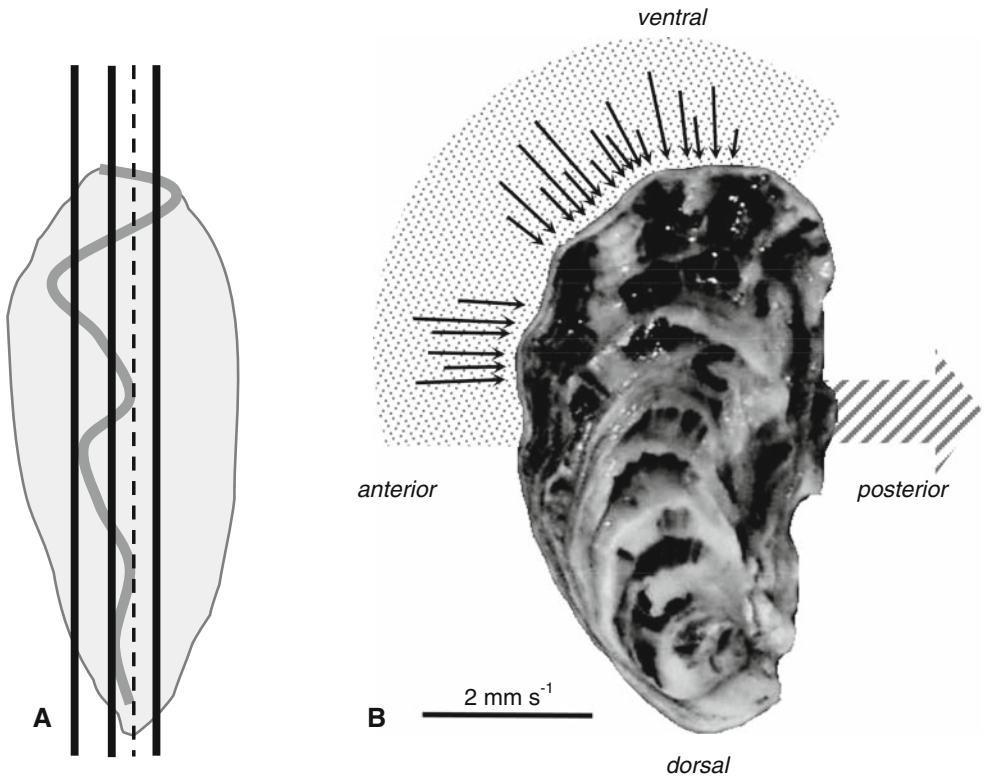


**Fig. 1** Indication of the different laser sheet projections (**a**) used to determine the area of in- and outflow in *C. gigas* (**b**). **a** The frontal view of an oyster, showing both valves and undulating shell edges. The *dashed line* indicates the sagittal plane. Different projections of the laser-sheet, parallel to the sagittal plane, are indicated as *black lines*. **b** Areas of in- and outflow in a Pacific oyster. The *dotted area* is the inflow area, and the *hatched arrow* indicates the location and direction of the exhalant flow. *Arrows* in the inflow area indicate inhalant current velocities determined in the DPIV analysis. The *length of an arrow* indicates its magnitude, according to the *scale bar* below

upright in the black grit (Fig. 2c). This is a natural orientation for oysters in dense oyster beds. Larger oysters were placed horizontally, lying on their cupped valve. The dorsal end of the shell was resting on a mound of grit, thereby creating sufficient distance between the gape at the ventral end of the shell and the bottom of the tank to ensure an unobstructed flow field.

To facilitate a comparison between the three species, we determined inhalant current velocities at the entrance of the furthest protruding structure: in *C. gigas* at the shell entrance (the mantle entrance was not always visible and never protruded beyond the shell entrance), in *M. edulis* at the mantle entrance, and in *C. edule* at the siphon entrance (point of inflow, Fig. 2d–f). The experimental animals were kept no longer than 4 h in the set-up, including acclimation time, and were then returned to their tank with clean seawater (without synthetic particles) and algae.

Flow fields and inhalant current velocities were studied in seven individual specimens for *C. gigas*, seven for *M. edulis* and eight for *C. edule*. Per individual, 5–10 sequences were recorded during periods of active pumping (when seeding particles were observed to be sucked in with relatively high speeds). In the DPIV analysis, one pair of filmed frames was analyzed per sequence (selected visually). Overview flow fields were exported to a spreadsheet to analyse velocity profiles.

Because DPIV cannot resolve velocities closest to the animal (Frank et al. 2008), inhalant feeding current velocities at the inhalant aperture were analyzed in more detail using PTV. Single particles were tracked (using Didge© 2.3b1 by A. J. Cullum, Creighton University, Omaha, NE, USA) by manually pointing out corresponding particles in the same digital images series as used for the DPIV analysis. Changes in displacement in $x$ and $y$ direction were calculated, and from these, particle velocities that represent water current velocity. Per individual bivalve, five sequences of $\geq$20 frames were analyzed in Didge. Per sequence, at least five particles were tracked.

Upon completion of the experiments, the experimental animals were dried and incinerated to determine the ash-free dry weight of their flesh. The flesh was dried for 3 days at 70°C and incinerated at 550°C for 4 h. Mean current velocities at the inhalant aperture were related to ash-free dry body weight per individual.

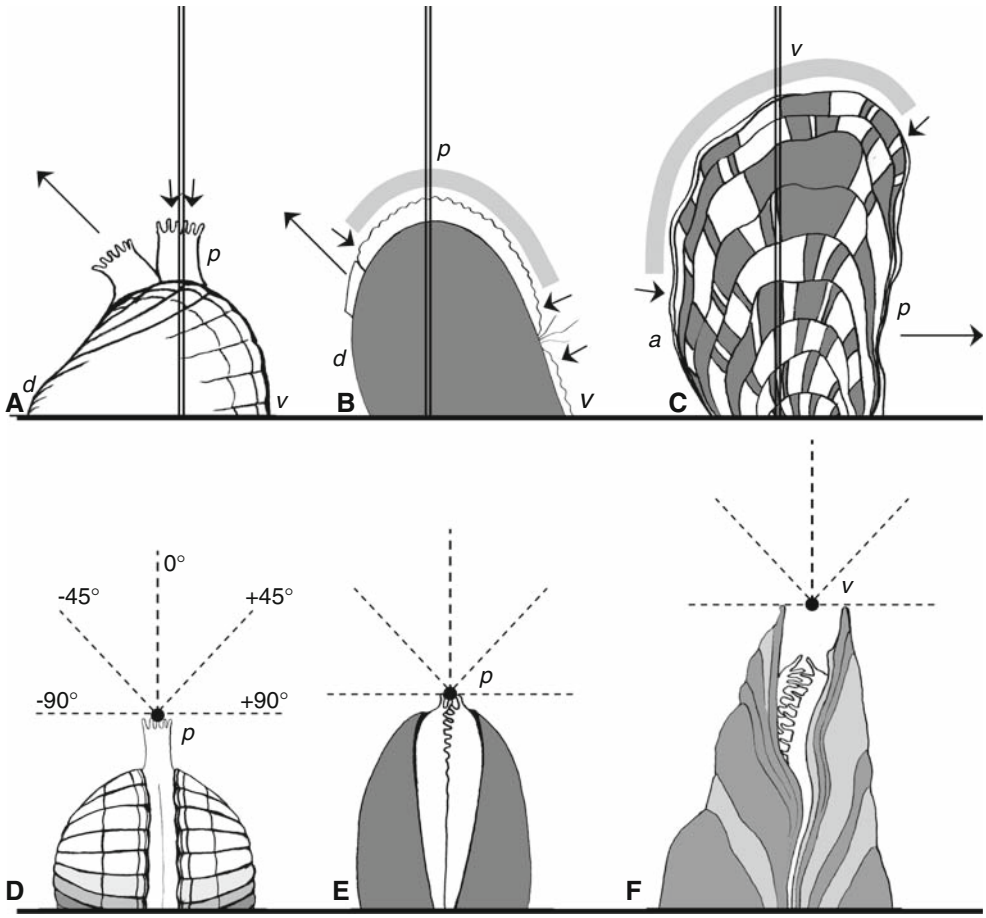


**Fig. 2** The orientation of the three species in the DPIV set-up, indicating the cross-sectional plane of the laser sheet: **a** *C. edule*, **b** *M. edulis*, **c** *C. gigas* and the orientation of transects along which velocity gradients were studied: **d** *C. edule*, **e** *M. edulis*, **f** *C. gigas*. In **a–c**, the inhalant areas are indicated with *short arrows*. A larger inflow area (**b–c**) is indicated as a *grey area* between these *arrows*. The exhalant jet is depicted as a *long arrow*. In **d–f**, the point of inflow (distance = 0) is marked with a *black dot*. $d$ = dorsal, $v$ = ventral, $a$ = anterior and $p$ = posterior

## Velocity profiles

The DPIV overview flow fields were processed to velocity profiles. Inhalant current velocities were related to the distance from the point of inflow along transects in the laser plane that cross-sectioned the sagittal plane perpendicularly (Fig. 2d–f). We compared velocity profiles from different directions towards the inhalant aperture, at angles of 0°, 45° and 90° relative to the sagittal plane of the bivalves (Fig. 2d–f). In *C. edule*, the point of inflow (distance = 0 mm) was localized at the centre of the tip of the inhalant siphon, in *M. edulis* at the centre of the inhalant aperture, at the same height as up to where the mantle protruded, and in *C. gigas* at the centre of the inhalant aperture, at the same height as up to where the shell valves protruded (Fig. 2d–f). All velocity profiles for each individual and each transect were processed to scatter graphs (Sigmaplot® 2001) and curves representing exponential decay with distance were fitted corresponding to the formula

$$v(r) = v_0 + a\mathrm{e}^{-br} \quad (1)$$

where $v$ (in mm $s^{-1}$) is the incurrent velocity at distance $r$ (in mm) from the point of inflow in the inhalant aperture, $v_0$ is the background velocity (that should be 0 mm $s^{-1}$ in still water), and '$a$' and '$b$' are constants. Constant '$a$' describes the maximum inflow velocity at $r = 0$ mm due to the pumping activity of the animal. Constant '$b$' is the acceleration coefficient: it describes the slope of the curve, and thereby the acceleration of the inhalant feeding current towards the point of inflow. Acceleration coefficients were compared between species.

Feeding currents can be considered to influence the surrounding water up to the distance where $v$ becomes $v_0$. Because of the asymptotical nature of Eq. 1, $v$ can never become $v_0$, but only approaches this value. According to

Eq. 1, if $v$ approaches $v_0$, $ae^{-br}$ approaches 0. We chose to calculate the distance of influence $d_{infl}$ from $ae^{-br} = 0.01$ mm $s^{-1}$, and thus from the following formula (modified from Eq. 1).

$$d_{inf1} = -\ln(0.01/a)/b \quad (2)$$

The distance of influence $d_{infl}$ along the 0° transect parallel to the sagittal plane was calculated per individual, using the average '$a$' and '$b$' values of all analyzed sequences, and compared between species.

The velocity profile of the half-buried *C. edule* in our set-up will be different from the field where cockles are generally buried completely in the sediment. We applied a mathematical correction to compensate for this difference. In half-buried *C. edule*, iso-velocity surfaces will be approximately sphere-shaped (with some interference from the animal itself), but for a completely buried cockle the iso-velocity surfaces would be in the shape of a hemisphere (André et al. 1993). When comparing a sphere and a hemisphere with the same (filtered) volume, the radius of the hemisphere is 1.26 times larger than the radius of the full sphere (according to the formula to calculate the volume of a sphere: $^4/_3\ \pi$ radius$^3$). Since the inflow velocity remains the same, the distance of influence will be 1.26 times larger and the acceleration coefficient will be 1.26 times smaller if the cockles are buried. Hence, we multiplied both parameters with correction factors 1.26 and 1/1.26, respectively.

## Exhalant jets

The location and direction of the exhalant jets were determined visually. This was facilitated by the efficient retention of the Pliolyte particles on the bivalve gills, resulting in an excurrent jet of particle-depleted water that was clearly visible in the particle seeded field. However, the empty exhalant jet did not allow for direct current-velocity analyses. High-velocity particles are visible just adjacent to the jet, but these are entrained particles, accelerated by the shear of the jet. Although exhalant jet speeds may be reconstructed using spline interpolation (Spedding and Rignot 1993; Stamhuis et al. 2002), this will introduce an additional error (Frank et al. 2008 and note the in this context complicating bifurcated exhalant jet). Rather, we chose to estimate average exhalant jet speeds using a mathematical model. Average jet speeds (in cm $s^{-1}$) were calculated as $Q/A_{exh}$ with $Q$ being the volume flux (pumped volume of water; in $cm^3\ s^{-1}$) and $A_{exh}$ being the cross-sectional area of the exhalant aperture (in $cm^2$). For $Q$ we used a range of filtration rates from literature. $A_{exh}$ was determined from the frames that were recorded for the DPIV and PTV analyses by measuring the exhalant siphon diameters from dorsal and lateral recordings. During recording, additional images have been recorded that allowed for measurements of exhalant apertures and shell gapes. In *C. edule*, $A_{exh}$ was calculated as the surface area of a circle: as $\pi r^2$ with $r$ being the radius of the opening of the extended exhalant siphon. In *M. edulis* and *C. gigas*, $A_{exh}$ was calculated as an oval: as $\pi \times ½d_1 \times ½d_2$ with $d_1$ being the largest diameter (along the sagittal plane) and $d_2$ the smallest diameter (perpendicular to the sagittal plane). In *M. edulis*, these diameters were measured from dorsal recordings (camera flush with the sagittal plane) of upright mussels. In *C. gigas* the dimensions could not be measured directly since the exhalant aperture is located inside the shell. We assumed that the smallest diameter $d_2$ of the exhalant siphon was equal to the shell gape at the location of the exhalant aperture. The shell gape was determined from dorsal recordings (camera oriented flush with the sagittal plane). From lateral recordings with clearly distinguishable exhalant jets, the largest diameter $d_1$ of the exhalant aperture was estimated by measuring the width of the exhalant jet. Recorded sequences of three individual oysters were clear enough to allow for a reliable estimate of $d_1$. For these individuals, the ratio of $d_1$ to $d_2$ ranged from 1 to 2. Therefore, $d_1$ was assumed to range from $d_2$ to $2d_2$, and $A_{exh}$ was thus assumed to lie between $\pi \times ½d_2 \times ½d_2$ and $\pi \times ½d_2 \times d_2$. Jet speeds were modelled with $A_{exh}$ values calculated with both formulas, as upper and lower limits. Jet speeds were modelled for a range of filtration rates and a range of siphon cross-sectional areas, since both are variable with body weight, trophic conditions and other parameters (Newell et al. 2001, and references therein).

## Statistical analysis

Curve fitting and non-linear regression analysis were performed in Sigmaplot® 2001. All other statistical tests were performed in SPSS® 12.0.1. Data were visually checked for normality using a Q–Q plot, and for equality of variances by plotting studentized residuals against predicted values. Additionally, Levene's test for homogeneity of error variances was used. If the prerequisites were not met, the data were ln-transformed before testing. A significance level of $\alpha = 0.05$ was maintained. In testing differences between species with GLM in SPSS® 12.0.1. (aided by Norušis 2008), 'species' was always included as fixed factor, along with either 'shell length' or 'body weight' as covariate. Homogeneity of slopes was tested first, by including the effects of the fixed factor, the covariate, and the interaction term *fixed_factor*covariate* in the model. If slopes were equal (*fixed_factor*covariate*: $p > 0.05$), the full factorial model was tested to find differences between species (in intercepts). If significant differences in intercepts were found (*fixed_factor*: $p < 0.05$), multiple pair-wise

comparisons were performed (the same GLM analysis, three combinations of 2 species tested separately).

## Results

All experimental animals were observed to be filtering actively, cockles with open and extended siphons, mussels with open and extended mantles, and oysters with open and extended mantles inside the open shell. The animals appeared to be healthy and their behaviour normal. The seeding particles appeared not to hamper the filtration activity.

### Localizing inhalant apertures

Inhalant feeding-current velocities of *C. gigas* showed high small-scale fluctuations along the gape. This is probably due to the undulating form of the shell edges, causing different gape widths along the shell edge. Inflow occurred along a large part (appr. 30%) of the anterior to ventral gape (Fig. 1b). On a larger scale incurrent velocities did not differ considerably between different parts of the shell (e.g. the anterior and ventral parts).

Although for *M. edulis* incurrent velocities were highest in the area at the posterior end of the shell, inflow was observed along the entire ventral to posterior gape between somewhat below the byssal opening and the exhalant siphon. *C. edule* showed inhalant flow through the inhalant siphon. In some cases, however, the halfway buried cockles were occasionally observed to inhale water through the opening between both mantle folds that is normally used for extension of the foot, while still inhaling water through the inhalant siphon. Because the opening of this third aperture reduced the incurrent velocity in the inhalant siphon, and will not occur in fully buried cockles, such observations were excluded from further analysis.

### Inhalant feeding current velocities

In all three species, larger individuals generally showed higher inhalant current velocities than smaller individuals (Fig. 3). A relationship with shell length was significant for *C. gigas* ($p = 0.04$; Table 1) but not for *M. edulis* and *C. edule* (respectively, $p = 0.14$ and 0.08; Table 1). Relationships with body weight (g AFDW) were not significant (Table 1; $p = 0.05$ (*C. gigas*), 0.34 (*M. edulis*), 0.08 (*C. edule*). Although a significant effect of shell length and body weight was lacking in all cases but one, $p$ values in *C. gigas* and *C. edule* approached the significance level of 0.05. Therefore, an effect of both variables could not convincingly be rejected, and we included shell length and body weight as covariates in GLM analyses to test differences between species.

At comparable shell lengths, inhalant feeding-current velocities in *C. gigas* were significantly lower than inhalant feeding-current velocities in both *M. edulis* and *C. edule* (GLM tested with 'shell length' as covariate: equal slopes, but different intercepts; Table 2). Inhalant velocities in *M. edulis* were 5.05 mm $s^{-1}$ higher than in *C. gigas*, and in *C. edule* 7.31 mm $s^{-1}$ higher than in *C. gigas* (Table 3). No significant differences between species were found when tested with body weight as covariate (Tables 2, 3). Disregarding the (potential) effect of shell length and body weight, mean values of the acceleration coefficient '*b*' over the entire ranges of shell lengths and body weights did not differ between species (one-way ANOVA: $F = 0.17$, $p = 0.84$; for $N$ see Table 1).

### Velocity profiles

Acceleration coefficients of velocity profiles from different directions towards the point of inflow (Fig. 2), at angles of

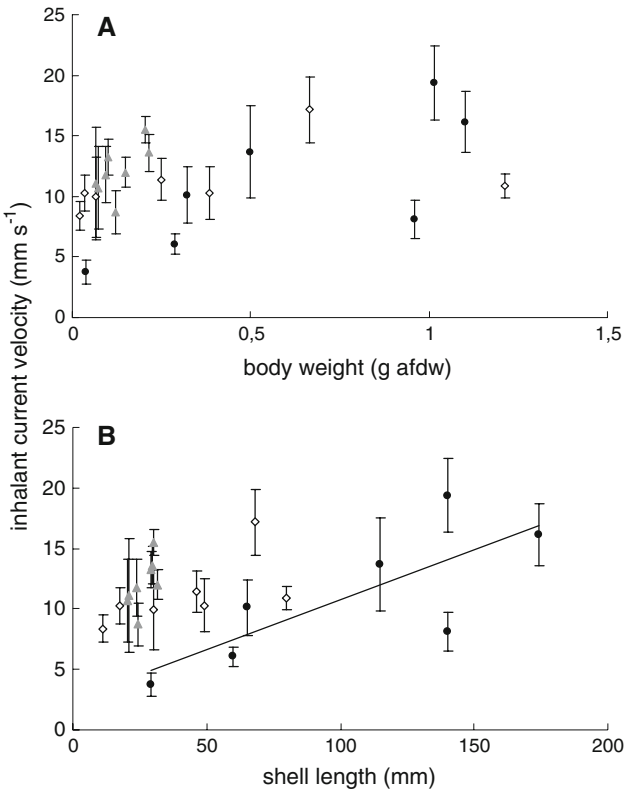


**Fig. 3** Mean inhalant feeding current velocities at the inhalant aperture per individual in mm $s^{-1}$ (with standard deviations), plotted against body weight (**a**) and shell length (**b**) for *C. gigas* (*black filled circles*), *M. edulis* (*open diamonds*) and *C. edule* (*grey filled triangles*). A regression line is drawn through inhalant feeding current velocities of *C. gigas*, plotted against shell length (**b**; linear regression: $R^2 = 0.60$, $p < 0.05$)

**Table 1** Results of linear regression analysis; for each bivalve species relationships of inhalant feeding current velocity, acceleration coefficient '*b*' and distance of influence $d_{infl}$ with shell length (mm) and body weight (g AFDW, ln-transformed) were tested

| Dependent | Species | *N* | *df* | Independent: shell length | | | Independent: body weight | | |
|---|---|---|---|---|---|---|---|---|---|
| | | | | $R^2$ | *F* | *p* | $R^2$ | *F* | *p* |
| Inhalant velocity | *C. edule* | 8 | 7 | 0.42 | 4.36 | 0.08 | 0.42 | 4.38 | 0.08 |
| | *M. edulis* | 7 | 6 | 0.38 | 3.01 | 0.14 | 0.18 | 1.1 | 0.34 |
| | *C. gigas* | 7 | 6 | 0.6 | 7.57 | 0.04 | 0.56 | 6.42 | 0.05 |
| '*b*' | *C. edule* | 8 | 7 | 0.6 | 8.98 | 0.02 | 0.47 | 5.37 | 0.06 |
| | *M. edulis* | 7 | 6 | 0.8 | 19.33 | 0.01 | 0.84 | 26.00 | 0.00 |
| | *C. gigas* | 6 | 5 | 0.21 | 1.07 | 0.36 | 0.56 | 5.07 | 0.09 |
| $d_{infl}$ | *C. edule* | 8 | 7 | 0.7 | 13.66 | 0.01 | 0.42 | 4.29 | 0.08 |
| | *M. edulis* | 7 | 6 | 0.6 | 7.34 | 0.04 | 0.64 | 8.72 | 0.03 |
| | *C. gigas* | 6 | 5 | 0.19 | 0.92 | 0.39 | 0.58 | 5.45 | 0.08 |

Sample sizes (*N*), degrees of freedom (*df*), $R^2$, *F* and *p* values are given. Significant relationships ($p < 0.05$) are underlined

**Table 2** Differences in inhalant feeding-current velocity and the velocity-profile parameters '*b*' (acceleration coefficient) and $d_{infl}$ (distance of influence) between three species of bivalves; statistical results of GLM with 'species' as fixed factor and either 'shell length' (mm) or (ln-transformed) body weight (g AFDW) as covariate

| | GLM | | | | | |
|---|---|---|---|---|---|---|
| | Covariate = shell length | | | Covariate = body weight | | |
| | *df* | *F* | *p* | *df* | *F* | *p* |
| Inhalant velocity | | | | | | |
| Slopes (effect of *species*covariate*) | 2 | 0.50 | 0.62 | 2 | 2.07 | 0.16 |
| Intercepts (effect of *species*) | 2 | 6.71 | 0.01 | 2 | 2.4 | 0.12 |
| '*b*' | | | | | | |
| Slopes (effect of *species*covariate*) | 2 | 7.76 | 0.01 | 2 | 1.08 | 0.36 |
| Intercepts (effect of *species*) | 2 | nt | nt | 2 | 14.76 | 0.00 |
| $d_{infl}$ | | | | | | |
| Slopes (effect of *species*covariate*) | 2 | 8.24 | 0.00 | 2 | 2.67 | 0.10 |
| Intercepts (effect of *species*) | 2 | nt | nt | 2 | 6.73 | 0.01 |

Degrees of freedom (*df*), *F* and *p* values are given. Where significant differences in slopes or intercepts between the regression lines for the three species were found, *p* values are underlined. Sample sizes (*N*) per species are given in Table 3

*nt* not tested since the prerequisite homogeneity of slopes was not met

0°, 45° and 90° relative to the sagittal plane of the bivalves, were not significantly different (Friedman test, Table 4). Therefore, we continued our analysis of velocity profiles along transects at an angle of 0° only.

For *C. gigas*, one individual that yielded extreme values for '*b*' (0.075) and $d_{infl}$ (75.8 mm) (Fig. 4), as revealed by a simple boxplot, was removed from further analysis. This reduced the sample size to 6 for oysters (Table 3).

In *C. gigas*, the velocity profile parameters '*b*' and $d_{infl}$ showed no relationship with either shell length or body weight (Table 1; Fig. 4). For the other two species we did find significant relationships. The acceleration coefficient '*b*' decreased linearly with shell length in *M. edulis* and *C. edule*, and logarithmically with body weight (ln-transformed in linear regression analysis) in *M. edulis* (Table 1; Fig. 4). The distance of influence $d_{infl}$ increased linearly with shell length in *M. edulis* and *C. edule*, and logarithmically with body weight (ln-transformed in linear regression analysis) in *M. edulis* (Table 1; Fig. 4). Because both shell length and body weight affect velocity profile parameters in at least two of the three species (note also the low *p* values in non-significant regressions), we included these variables as covariates in GLM analyses to test differences in '*b*' and $d_{infl}$ between species.

After correction of results for *C. edule* for not being buried completely (Table 3), the acceleration coefficient '*b*' was significantly higher for *C. gigas* than for both *M. edulis* and *C. edule* at comparable body weight (Tables 2, 3). Acceleration coefficients for *M. edulis* and *C. edule* were, respectively, 0.27 and 0.33 lower than for *C. gigas* (Table 3). Testing differences between species with shell length as covariate yielded no results since the

**Table 3** Differences in inhalant feeding-current velocity and the velocity-profile parameters '*b*' (acceleration coefficient) and $d_{infl}$ (distance of influence) between three species of bivalves; results of GLM (descriptives and parameter estimates) tested with 'species' as fixed factor and either 'shell length' (mm) or (ln-transformed) body weight (g AFDW) as covariate (see *F* and *p* values in Table 2)

| | *C. edule* | *M. edulis* | *C. gigas* |
|---|---|---|---|
| Inhalant velocity | | | |
| Mean | 12.08 | 11.18 | 11.03 |
| Standard error | 0.73 | 1.06 | 2.12 |
| *N* | 8 | 7 | 7 |
| GLM: intercepts (shell length) | 7.31[a] | 5.05[a] | 0.00[b] |
| GLM: intercepts (body weight) | 4.10 | 1.62 | 0.00 |
| '*b*' | | | |
| Mean (*C. edule* uncorrected) | 0.34 (0.43) | 0.37 | 0.53 |
| Standard error | 0.05 | 0.09 | 0.06 |
| *N* | 8 | 7 | 6 |
| GLM: intercepts (shell length) | na | na | na |
| GLM: intercepts (body weight) | −0.33[a] | −0.27[a] | 0.00[b] |
| $d_{infl}$ | | | |
| Mean (*C. edule* uncorrected) | 21.04 (16.70) | 25.68 | 13.24 |
| Standard error | 2.27 | 7.58 | 1.24 |
| *N* | 8 | 7 | 6 |
| GLM: intercepts (shell length) | na | na | na |
| GLM: intercepts (body weight) | 16.05[a] | 19.00[a] | 0[b] |

Mean values and standard errors are given. For *C. edule*, mean values of '*b*' and $d_{infl}$ are corrected for not being buried completely in the experiments (uncorrected means between brackets). The estimates of intercepts are relative. Intercepts for *C. gigas* are set at zero, and intercepts for the other species are given relative to *C. gigas*' intercepts. Significant differences between intercept, tested in multiple pair-wise comparisons, are given with lowercase letters in superscript

*na* not available; the difference in intercepts was not tested since the prerequisite homogeneity of slopes was not met (Table 2)

**Table 4** Differences between acceleration coefficients '*b*' of velocity profiles in three directions (0°, 45° and 90°); results of the Friedman test for multiple-related samples, tested for each species separately

| | *C. edule* | *M. edulis* | *C. gigas* |
|---|---|---|---|
| $\chi^2$ | 1.33 | 1.6 | 4.67 |
| *N* | 6 | 5 | 9 |
| *df* | 2 | 2 | 2 |
| *p* | 0.51 | 0.45 | 0.10 |

No significant differences were found

slopes of the regression lines were significantly different (Table 2). Disregarding the (potential) effect of shell length and body weight, mean values of '*b*' over the entire ranges of shell lengths and body weights did not differ between species (one-way ANOVA: $F = 2.15$, $p = 0.15$; for *N* see Table 1).

After correction of *C. edule* results for not being buried completely, $d_{infl}$ (the distance where $v = v_0 + 0.01$) was significantly smaller for *C. gigas* than for both *M. edulis* and *C. edule* at comparable body weight (Tables 2, 3). Distances of influence $d_{infl}$ for *M. edulis* and *C. edule* were, respectively, 19.00 and 16.05 mm larger than for *C. gigas* (Table 3). Testing differences between species with shell length as covariate yielded no results since the slopes of the regression lines were significantly different (Table 2). Disregarding the (potential) effect of shell length and body weight, mean values of $d_{infl}$ over the entire ranges of shell lengths and body weights did not differ between species (one-way ANOVA: $F = 1.66$, $p = 0.22$; for *N* see Table 1).

Velocity profiles of all three species, modelled with Eq. 1 and '*b*' and inhalant feeding-current velocities at the aperture (mean values for all individuals per species), are shown in Fig. 5. The velocity profile of *C. gigas* is steeper and has a smaller distance of influence compared to *M. edulis* and *C. edule*.

## Exhalant jets

Exhalant jets were distinctly visible as particle-depleted plumes in a particle-seeded field. In *C. gigas*, exhalant jets originated from the posterior region of the oyster (near the anus) in horizontal direction (Fig. 6a). In upright mussels in our set-up (oriented as in Fig. 2b) the exhalant jet was directed away from the bottom (Fig. 6b), roughly at an angle of 50°–70° relative to the bottom. The mussels appeared to be capable of modifying the direction of the exhalant jet somewhat relative to the shell. In *C. edule*, the exhalant jet was directed vertically and away from the bottom (Fig. 6c).

The cross-sectional area of the exhalant aperture $A_{exh}$ ranged from 0.03 to 0.08 $cm^2$ in *C. edule*, from 0.003 to 0.16 $cm^2$ in *M. edulis* and, as estimated, from 0.001 to 0.28 $cm^2$ in *C. gigas* (Table 5). $A_{exh}$ increased with shell length and body weight in *M. edulis* and *C. gigas*, but showed no relationship with both variables in *C. edule* (non-linear regression; Table 6).

A range of filtration rates (*Q*) was derived from literature; these ranged from approximately 1.0 to 5.0 l $h^{-1}$ in *C. edule* (Vahl 1972; Foster-Smith 1975; Møhlenberg and Riisgård 1979), from 1.5 to 6.0 l $h^{-1}$ in *M. edulis* (Walne 1972; Riisgård 1977; Møhlenberg and Riisgård 1979) and from 3.8 to 12.5 l $h^{-1}$ in *C. gigas* (Walne 1972; Gerdes 1983; Bougrier et al. 1995) (Table 5) in animals of different sizes and measured under different experimental conditions (see cited papers).

Jet speeds were calculated using average values of $A_{exh}$ and *Q* (Table 5). Average jet speeds were thus calculated to be 20.8 cm $s^{-1}$ in *C. edule*, 18.5 cm $s^{-1}$ in *M. edulis* and

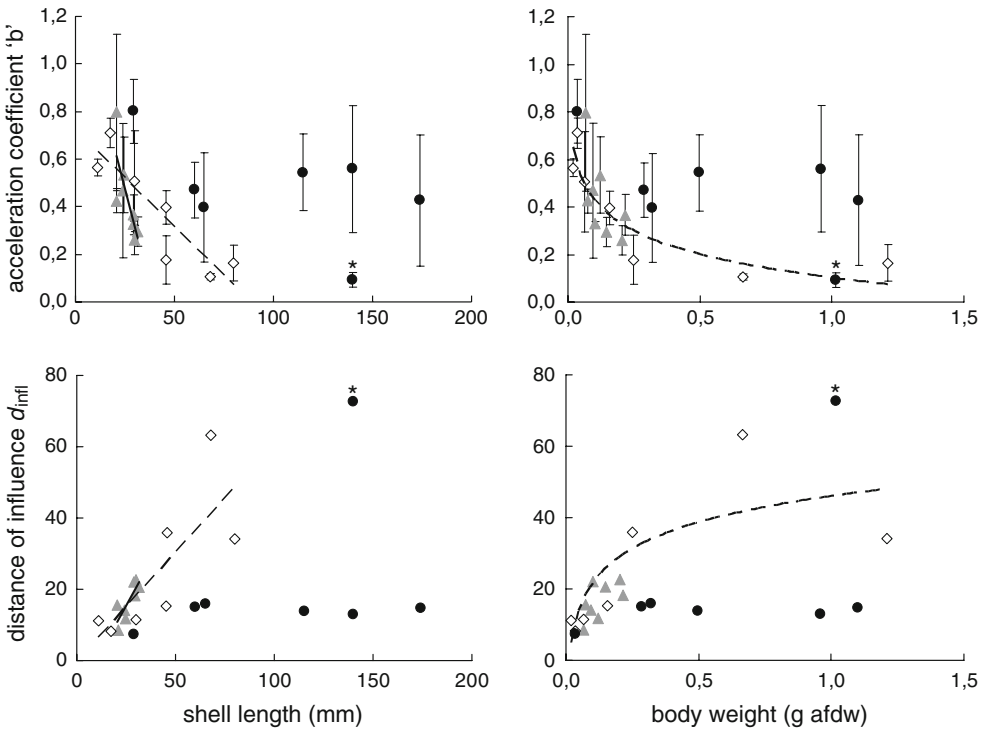


**Fig. 4** Acceleration coefficient and distance of influence plotted against shell length and body weight for *C. edule* (*grey triangles*), *M. edulis* (*open diamonds*), and *C. gigas* (*black circles*). *Error bars* represent standard deviations. Significant trendlines [(non)linear regression: $p < 0.05$] are drawn for *C. edule* (*solid line*; shell length: '*b*': $R^2 = 0.60$; $d_{infl}$: $R^2 = 0.69$) and *M. edulis* (*dashed line*; shell length: '*b*' linear: $R^2 = 0.79$, $d_{infl}$ linear: $R^2 = 0.59$; body weight: '*b*' logarithmic: $R^2 = 0.84$, $d_{infl}$ logarithmic: $R^2 = 0.64$). Extreme values for *C. gigas* that were excluded from statistical analysis (GLM) are indicated with an *asterisk*

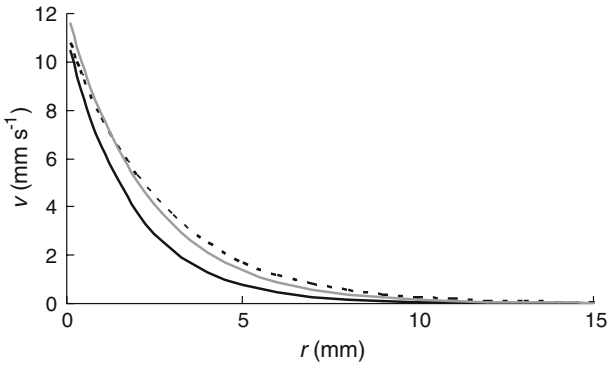


**Fig. 5** The average velocity profiles in the inhalant flow fields of *C. gigas* (*solid black line*), *M. edulis* (*dashed black line*) and *C. edule* (*solid grey line*), representing an exponential decay of the inhalant current velocity $v$ with distance $r$ from the inhalant aperture. The curves are based on Eq. 1, but without background current $y_0$: $v(r) = ae^{-br}$, with the mean '*a*' and '*b*' parameters per species used as input

24.3–48.6 cm $s^{-1}$ (calculated with upper and lower estimates for $A$, see "Materials and methods") in *C. gigas*. Since $A_{exh}$ and $Q$ are both variable parameters, jet speeds were also modelled for a range of both parameters. When modelling a range of $A_{exh}$, $Q$ was kept constant at average values, as derived from literature, of 3.0 l $h^{-1}$ for *C. edule*, 4.0 l $h^{-1}$ for *M. edulis* and 7.0 l $h^{-1}$ for *C. gigas*. When modelling a range of $Q$, $A_{exh}$ was kept constant at average values, as measured and estimated in this study over a range of body weight per species, of 0.04 for *C. edule*, 0.06 for *M. edulis* and for *C. gigas* 0.04 (upper limit) and 0.08 (lower limit). Figure 7 illustrates how the jet speed in all three species varies with $A_{exh}$ and $Q$. With increasing $A_{exh}$ but constant $Q$, jet speeds decreased. Because of the higher filtration rate in *C. gigas*, its modelled jet speeds are higher at similar cross-sectional areas of exhalant apertures. With increasing $Q$ but constant $A_{exh}$, modelled jet speeds increased. Jet speeds of *M. edulis* were within the range of jet speeds estimated for *C. gigas*. Jets speeds in *C. edule* were equal to the upper estimated limit of *C. gigas* at similar filtration rates, but because *C. gigas* display wider ranges in filtration rate (due to a larger natural range in body weight and its relationship with filtration rate, for the latter see Møhlenberg and Riisgård 1979), over the entire range *C. gigas* may show higher jet speeds.

## Discussion

### Methodological considerations

Performing the experiments in still water did not exclude background water currents completely. The strong exhalant jets caused disturbance of water movement in inhalant flow fields when located nearby, especially in cockles, and when reflected by the nearby tank wall. The exhalant jets in general caused some slight background circulation that was in most cases well below 1 mm $s^{-1}$ in different directions (measured with DPIV). Recordings with higher background currents were excluded from the analysis.

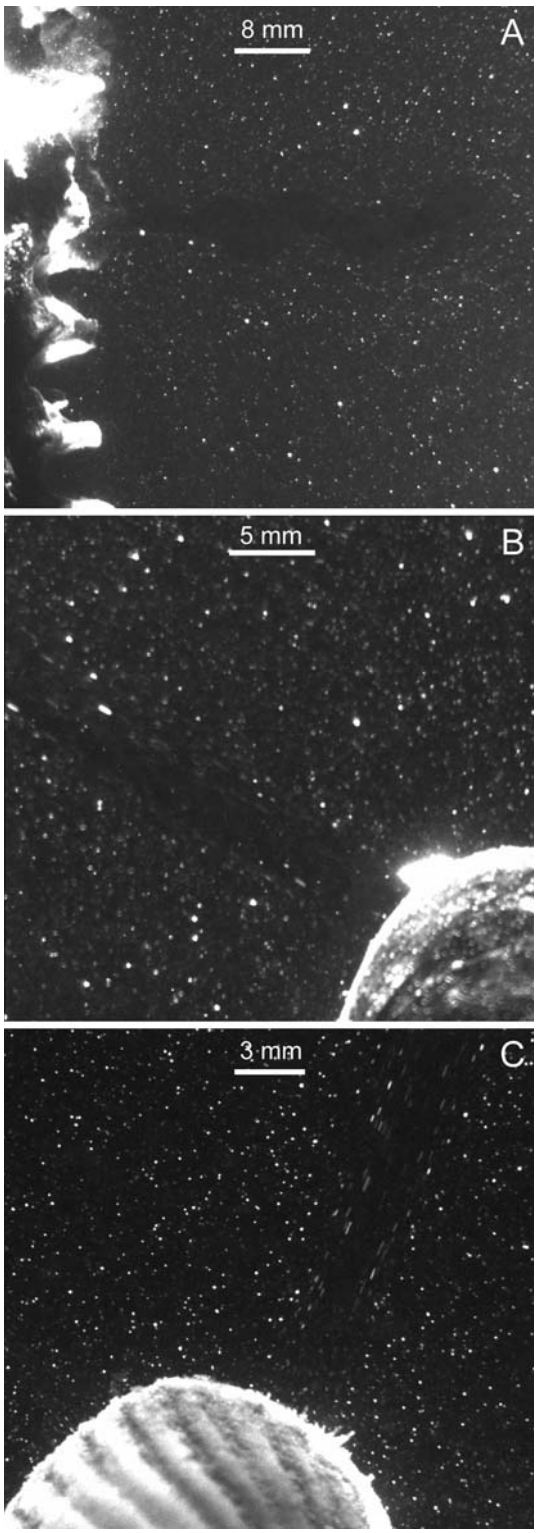


**Fig. 6** Exhalant jets in *C. gigas* (**a**), *M. edulis* (**b**) and *C. edule* (**c**). These are filmed frames. The *white specks* are synthetic particles, illuminated by the laser sheet. The exhalant jets are visible as *dark plumes*, flanked by *white streaks* that are fast moving particles in the surrounding water dragged along with the exhalant jet

Variations in inhalant feeding-current velocities between and within species were high. This may be caused by small variations in siphon diameter, valve gape and mantle gape, and by local variations along the irregularly shaped shell and mantle edges of *C. gigas* and mantle of *M. edulis*. Additionally, the animals may have adjusted their clearance rates to short-term fluctuations in particle and algal concentrations caused by the continuous depletion by the bivalves' filtration activity and periodical replenishments (Hawkins et al. 2001; Riisgård et al. 2003).

Exhalant jet speeds could not be measured directly because the particles used to visualize water movement were retained efficiently by the bivalve gills. Frank et al. (2008) solved this problem by using particles that were too small (about 2 μm) to be retained efficiently by the gills in measuring exhalant jet speeds of several bivalve species using DPIV. With the magnification used in our set-up, such small particles would not have been visible, particularly at the highest water-current velocities measured.

## Inhalant flow field

In *M. edulis*, mean inhalant feeding-current velocities at the inhalant aperture ranged up to 17.2 mm $s^{-1}$ (68 mm shell length). Green et al. (2003) measured inhalant feeding-current velocities in *M. edulis* (22.6–23.7 mm shell length) of up to 6 mm $s^{-1}$ at a slight distance from the gape (<1 mm), at 17°C by tracking particles. We found higher inhalant current velocities at the inhalant aperture itself, but the modelled velocity profiles (Fig. 5) show a velocity of 7.7 mm $s^{-1}$ at a distance of 1 mm from the aperture, corresponding to the results by Green et al. (2003).

In *C. gigas* of 9.0–11.0 cm shell length, at a seawater temperature of 12–14°C, Tamburri et al. (2007) found a mean inhalant current velocity of $1.65 \pm 0.10$ (SE) mm $s^{-1}$ at a distance of $\sim$1.5 mm from the gape. We found much higher inhalant feeding current velocities for a *C. gigas* individual of similar size: for an oyster of 11.5 cm shell length, we found an inhalant feeding current velocity of 13.7 mm $s^{-1}$ at the inhalant aperture, that had decreased according to the velocity profile for this individual to 8.6 mm $s^{-1}$ at a distance of 1.5 mm from the inhalant aperture. We also found a larger distance of influence in *C. gigas* than Tamburri et al. (2007) did. For *C. gigas* kept in still water, Tamburri et al. (2007) observed an influence of inhalant feeding currents at distances of 1–2 mm from the gape, but not at distances of 4–20 mm. For the same species, we found distances of up to 13.2 mm on average where the inhalant velocity had decreased to 0.01 mm $s^{-1}$. Differences in inhalant current velocity and distance of influence may be partially due to a difference in

**Table 5** Values for $A_{exh}$ (measured and estimated cross-sectional areas of the exhalant aperture, in $cm^2$) and FR (filtration rates derived from literature, in l $h^{-1}$ individual$^{-1}$) that were used to calculate exhalant jet speeds for all three species

| Species | $A_{exh}$ ($cm^2$) | FR (l $h^{-1}$) | Jet speed (cm $s^{-1}$) |
|---|---|---|---|
| *Cerastoderma edule* | 0.04 (0.03–0.08) | 3.0 (1.0–5.0) | 20.8 |
| *Mytilus edulis* | 0.06 (0.003–0.16) | 4.0 (1.5–6.0) | 18.5 |
| *Crassostrea gigas* | 0.04–0.08 (0.001–0.28) | 7.0 (3.8–12.5) | 24.3–48.6 |

Mean values are given, with ranges in brackets. Expressed in $cm^3$ $s^{-1}$, FR was used as $Q$ (volume flux) to calculate exhalant jet speeds (in cm $s^{-1}$) according to the formula: jet speed = $Q/A$

**Table 6** Results of non-linear regression analysis of relationships between exhalant siphon area $A_{exh}$ and either shell length (mm) or body weight (g AFDW) as independent factors according to the equations $A_{exh} = a$ (independent)$^b$ ($a$ and $b$ are constants)

| Independent | Species | $N$ | $R^2$ | $F$ | $b$ | $p$ |
|---|---|---|---|---|---|---|
| Shell length | *C. edule* | 8 | 0.32 | 2.80 | | 0.15 |
| | *M. edulis* | 10 | 0.83 | 38.21 | 1.56 | 0.00 |
| | *C. gigas* | 9 | 0.67 | 14.32 | 3.35 | 0.01 |
| Body weight | *C. edule* | 8 | 0.23 | 1.81 | | 0.23 |
| | *M. edulis* | 10 | 0.83 | 39.42 | 0.65 | 0.00 |
| | *C. gigas* | 9 | 0.69 | 15.29 | 0.86 | 0.01 |

Significant relationships ($p < 0.05$) are underlined

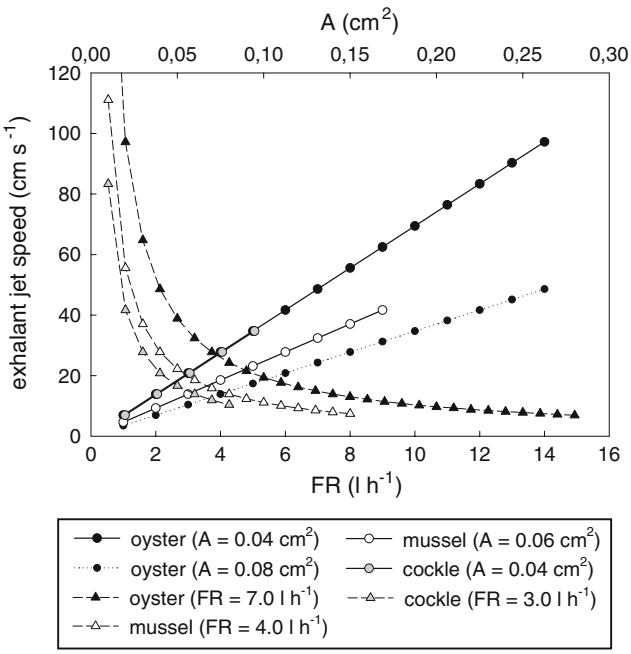


**Fig. 7** Model calculations on exhalant jet speeds (in cm $s^{-1}$) in *C. gigas*, *M. edulis* and *C. edule*, with varying exhalant-aperture cross-sectional area ($A$, in $cm^2$) and filtration rate (FR, in l $h^{-1}$)

methodology. Tamburri et al. (2007) injected a 1 µl bolus of a neutrally buoyant dye at different distances from the gape and analyzed the velocity in the initial 5-s interval after injection. A speed as minimal as 0.01 mm $s^{-1}$, more or less arbitrarily chosen in our study to facilitate a comparison of $d_{infl}$ between species, may be very difficult to detect with a method such as Tamburri et al. (2007) used. Differences may also have been induced by a difference in experimental temperature. *C. gigas* increase their filtration rate with increasing temperature up to a maximum at about 19°C (Bougrier et al. 1995). The higher temperature used in our study (18°C) than in the study of Tamburri et al. (2007; 12–14°C) may have induced a larger filtration rate (Walne 1972) and subsequently higher inhalant current velocities and a larger $d_{infl}$ (Eq. 1). Additionally, it is also possible that differences in condition, origin of the animals, food concentrations and the food type used in the experiments caused differences in filtration activity.

André et al. (1993) measured inhalant current velocities in *C. edule* with 15–43 mm shell length of up to 12 mm $s^{-1}$ at 17°C, for one individual even up to 22 mm $s^{-1}$, by tracking particles. This corresponds well with our results. We found inhalant feeding current velocities ranging up to 15.5 mm $s^{-1}$ at the inhalant aperture in *C. edule* (of 30 mm shell length). The mean distance of influence of 21.0 mm (corrected for not being buried completely) of the inhalant flow field of *C. edule* corresponds to results for another cockle species. Ertman and Jumars (1988) observed influence of the inhalant siphon of *Clinocardium nuttallii* (Conrad) up to a distance of 10–20 mm vertically. These observations were made in a flume tank at a current velocity of 2.8 cm $s^{-1}$ (free-stream velocity), and the observed distance of influence of 10–20 mm was therefore likely smaller than it would have been in still water (Ertman and Jumars 1988; André et al. 1993).

No significant relationships between inhalant current velocities and body weight were found, and a significant relationship with shell length only in *C. gigas*. The $p$ values for the linear regression of inhalant feeding-current velocities with body weight and shell length in *C. edule* and *C. gigas* were close to 0.05 (Table 1). We could therefore not dismiss a potential relationship of inhalant feeding current velocity with body size in testing differences between species. Our results suggest that the filtration rate (FR or $Q$) increased faster with body size

than the inhalant aperture area $A_{inh}$, resulting in an increase in inhalant feeding-current velocity. However, both gill area and pumping rate approximately scale with length$^2$ and with weight$^{0.67}$ in many bivalve species (*M. edulis, C. edule* and 11 other species of suspension feeding bivalves, Møhlenberg and Riisgård 1979; Jones et al. 1992). Inhalant aperture area, being a two-dimensional variable, is also expected to scale with length$^2$ and with weigth$^{0.67}$, theoretically resulting in an equal rate of increase of $A_{inh}$ and $Q$ with body size, and therefore in a constant inhalant feeding-current velocity. In contrast with this theory, we found a significant relationship with shell length in *C. gigas* (Table 1; Fig. 3). Considering the large variation in our results, sample sizes may not have been large enough to detect positive trends with shell length or body weight in *C. edule* and *M. edulis*. A detailed study of allometric relationships would require close monitoring of valve gape, inhalant and exhalant-aperture areas, and filtration rates. This was, however, beyond the scope of our study.

The increase in the distance of influence with body size (Fig. 4) is probably a direct result of the decrease in acceleration coefficient (potentially in combination with an increase in inhalant feeding current velocity) in *M. edulis* and *C. edule*. The decrease of the acceleration coefficient with body size is more difficult to explain. It may be related to changes in the shape of the animal surrounding the inhalant aperture (Anayiotos et al. 1995), or to changes in aspect-ratio (length/width) of the inhalant aperture (Anayiotos et al. 1997). For a liquid with the same viscosity as blood, Anayiotos et al. (1997) showed that a higher aspect-ratio in an oval shaped orifice resulted in a steeper velocity profile. The same rule may apply to our results. The length of the inhalant aperture along the edge of the shell may be larger in *C. gigas* than in *M. edulis*, relative to the width of the inhalant aperture. Obviously, the ratio of length to width of the inhalant aperture of *C. gigas* is higher than the aspect-ratio of the circular inhalant aperture of *C. edule* ($\approx 1$). This theoretically agrees with the significantly lower acceleration coefficient of *C. edule* and *M. edulis* compared to *C. gigas*.

The influence of inhalant feeding currents of *C. edule* and *M. edulis* extends significantly further into the water column than the influence of inhalant feeding currents of *C. gigas* (Table 3; Fig. 4). In still water, a larger distance of influence may allow these species to forage in higher water layers than *C. gigas*, possibly resulting in a larger phytoplankton intake rate (Fréchette et al. 1989) at comparable near-bed phytoplankton concentrations and comparable filtration rates. However, still water is a rare occurrence in the vicinity of bivalve beds. Absolute differences between species were small, and potentially different effects on food flux towards the bivalves may be overwhelmed by turbulent boundary layer mixing in the field.

The significantly higher steepness of the inhalant velocity profile in *C. gigas* may have consequences for the entrainment of zooplankton species that can detect and escape from hydromechanical stimuli such as critical deformation rates and acceleration (Kiørboe and Visser 1999; Titelman and Kiørboe 2003). However, absolute differences in steepness were small between species and are not expected to lead to differences in the capture rate of zooplankton against background levels of turbulence caused by exhalant jets and shell roughness. The increased roughness of mussel beds and particularly oyster beds strongly increases near-bed turbulence and therefore ambient fine-scale deformation rates. Higher deformation rates in the inhalant feeding currents of *C. gigas* may therefore not have major negative impact of the capture rate of zooplankton. We did not, however, study hydromechanical stimuli (e.g. deformation rate) in the flow fields of the three species. Whether hydromechanical stimuli in the inhalant currents differ significantly from the ambient flow (and hence can be detected by potential prey items) can only be evaluated in flowing water.

In conclusion, the lower inhalant current velocity and smaller distance of influence and steeper velocity profile of the flow field of *C. gigas* may result in a reduced capacity to deflect larger particles, entrain slow-swimming zooplankton and forage from higher water layers. At comparable filtration rates this would imply a reduced ability to capture motile prey compared to *M. edulis* and *C. edule*. However, differences were found at comparable shell length and/or body weight. The natural size range of *C. gigas* is much larger than the natural size ranges of *C. edule* and *M. edulis*, and *C. gigas* can reach larger sizes and higher body weights. Therefore, when considering natural size ranges of the different species in the field, differences found are expected to be reduced (as an indication: one-way ANOVA gave no significant differences between mean inhalant feeding current velocities, '*b*', and $d_{infl}$ of the three species over the entire range of body sizes used). Furthermore, *C. gigas* individuals generally have higher filtration rates than *M. edulis* (Walne 1972) and *C. edule* (see "Introduction"; own unpublished results). Considering the relatively small differences found in inhalant feeding-current characteristics, differences in filtration rates are expected to be more determining for differences in food intake. Finally, potential differences in feeding efficiency as a result of small differences in inhalant feeding-current characteristics are expected to be overwhelmed by differences in food flux towards the bed due to differences in near-bed turbulence levels.

Exhalant jets

Modelled exhalant jet speeds were almost always higher in *C. gigas*, due to its higher filtration rate but similar cross-sectional area of the exhalant aperture. Although $A_{exh}$ was estimated and not measured directly for *C. gigas*, the order of magnitude should be reliable. The smallest diameter ($d_2$) of the exhalant aperture cannot have been wider than the shell gape. The largest diameter ($d_1$) of the exhalant aperture ranged from one to two times $d_2$, indicating a round to oval shaped exhalant aperture, as in *M. edulis* (Newell et al. 2001). Frank et al. (2008) measured a cross-sectional area of the exhalant aperture of 0.03–0.16 in *M. edulis* (51–62 mm shell length), which corresponds to our results. Highest exhalant jet speeds were determined at 4.06 cm $s^{-1}$ for *C. virginica*, 4.80 cm $s^{-1}$ for *Mercenaria mercenaria*, 12.31 cm $s^{-1}$ for *M. edulis* and 15.20 for *Argopecten irradians* (Frank et al. 2008). Their *M. edulis* were estimated to have filtered with a rate of 0.2 to 2.0 l $h^{-1}$. These values correspond well to our model results (Fig. 7). Newell et al. (2001) measured exhalant-aperture cross-sectional areas of 0.14–0.65 in large *M. edulis* individuals of 81.2 mm mean shell length. This is larger than what we measured, but so were the animals.

Although generally higher exhalant jet speeds were calculated for *C. gigas*, this does not necessarily mean a higher kinetic energy input in the benthic boundary layer. Kinetic energy input is determined by a balance between exhalant jet speeds and exhalant-aperture cross-sectional areas. The rate of transport of kinetic energy in a jet ($E$, in Watt) can be calculated as:

$$E = {}^1/_2\rho u^3 A \quad \text{(Tritton 1988)} \qquad (3)$$

where $\rho$ (kg $m^{-3}$) is the density of the medium, $u$ (m $s^{-1}$) is the average jet speed and $A$ ($m^2$) is the exhalant-aperture cross-sectional area (Tritton 1988). Using the average values measured and estimated for $A$, and average modelled jet speeds (both in Table 3), rates of kinetic energy transport in exhalant jets ($E$) of *C. edule* and *M. edulis* can be calculated to be approximately $2 \times 10^{-5}$ W. Rates of kinetic energy transport in exhalant jets of *C. gigas* appear, thus calculated, an order of magnitude higher: ranging from $6 \times 10^{-5}$ to $2 \times 10^{-4}$ W (for upper and lower limits of $A$ estimates).

Increased turbulent mixing inside and just above the bed enhances turbulent transport of phytoplankton towards the bivalves and thereby increases the food availability (Fréchette et al. 1989; Larsen and Riisgård 1997). At the same time, vertical exhalant jets reduce refiltration of already filtered water inside the bed (Jonsson et al. 2005; Widdows and Navarro 2007), and may blend near-bottom water, thereby increasing the thickness of the water layer available to suspension feeders (suggested by Larsen and Riisgård 1997). Bivalve suspension feeders can seriously deplete overlying phytoplankton concentrations (Dolmer 2000; Jonsson et al. 2005), which may lead to food-limited growth in dense beds (Kamermans 1993). Therefore, enhancing turbulent mixing probably contributes directly to enhanced growth. Regarding the higher modelled exhalant current velocities and the roughly estimated individual kinetic energy transfer only, *C. gigas* may affect near-bed turbulence levels through biomixing more strongly than *M. edulis* and *C. edule*. However, this may be counteracted by the different orientation of exhalant jets in *C. gigas* compared to the native species. Exhalant jets of *C. edule* are directed vertically and away from the bottom. In the field, exhalant jets in *M. edulis* are mostly directed away from the bed at angles varying roughly from 40° to 90° relative to the bottom (Maas Geesteranus 1942). Exhalant jets of *C. gigas* are not directed away from the bed but horizontally, parallel to the bottom (for oysters growing upright in beds on soft sediments as well as oysters living attached to hard substrates with their cupped valve; pers. obs.). This suggests a certain level of refiltration inside the oyster bed, which may reduce the food intake rate but may also be counteracted by the relatively large filtration rate of *C. gigas* individuals.

Besides through biomixing, epibenthic bivalves also affect turbulence levels by their physical presence on the sediment (Fréchette et al. 1989). Mussel beds and oyster reefs represent large biogenic roughness structures that may enhance near-bed turbulence levels significantly (Nikora et al. 2002). The effect of topographic roughness on turbulence is often assumed to scale with the length of the roughness structures (Butman et al. 1994; Van Duren et al. 2006 and references therein). In a closely packed experimental mussel patch (1,800 mussels $m^{-2}$), the average roughness height was estimated at 25–30 mm, as the difference between the lowest and the highest point of the mussel bed (Van Duren et al. 2006). Roughness height in an oyster bed is roughly in the order of 10–20 cm (own observations from the Oosterschelde estuary, SW Netherlands), which is an order of magnitude larger than in mussel beds. Because cockles cause bioturbation of sediments, they do affect bottom topography, but to a much smaller extent than mussels and oysters (Ciutat et al. 2007). Increased topographic roughness in a cockle bed, compared to similar sediment without cockles is in the order of a few mm at most (Fernandes et al. 2007). The difference in roughness height therefore seems more determining for potential differences in near-bed turbulence levels, food flux towards the bed, and entrainment of zooplankton prey. Because cockles hardly increase mixing by physical roughness, increased mixing due to exhalent jets (Ertman and Jumars 1988) may be more relevant to them, as may be optimizing the distance of influence of the inhalant flow field.

## Conclusions—implications for food intake

Our study shows that differences in inhalant feeding currents on the scale of equal-sized individual bivalves are small despite apparent differences in morphology between the species. Differences in inhalant feeding currents may even diminish when considering the natural size ranges of the species studied. Modelled exhalant jets of *C. gigas* were generally stronger than jets of native bivalves. This seems to result in a higher kinetic energy input in the boundary layer by individual oysters. However, implications of the horizontal orientation of the exhalant jets of *C. gigas* for food intake are unknown. We furthermore expect that the obviously large difference in roughness scale between beds of the invasive *C. gigas* and the native *M. edulis* and *C. edule* may be more relevant for potential differences in phytoplankton flux and zooplankton predation. Possible differences in food intake between the species should further be studied on the scale of a patch in the full range of biogenic interactions in a boundary flow.

**Acknowledgments** We are grateful to D. B. Blok, E. Brummelhuis, A. van Gool, J. J. de Wiljes and the crews of MS 'Valk' and MS 'Krukel' for their practical assistance. We thank P. Kamermans and anonymous reviewers for providing valuable comments on the manuscript. This project was funded by the Netherlands Organization for Scientific Research—Earth and Life Sciences (NWO-ALW) (project number 812.03.003). The experiments comply with the current Dutch laws.



## References

Anayiotos AS, Perry GJ, Myers JG, Green DW, Fan PH, Nanda NC (1995) A numerical and experimental investigation of the flow acceleration region proximal to an orifice. Ultrasound Med Biol 21:501–516. doi:10.1016/0301-5629(94)00141-Y

Anayiotos AS, Elmahdi AM, Newman BE, Perry GJ, Costa F, Agrawal D, Agrawal G, DeCarvalho CT, Nanda NC (1997) An improved flow evaluation scheme in orifices of different aspect ratios. Ultrasound Med Biol 23:231–244. doi:10.1016/S0301-5629(96)00228-1

André C, Jonsson PR, Lindegarth M (1993) Predation on settling bivalve larvae by benthic suspension feeders: the role of hydrodynamics and larval behaviour. Mar Ecol Prog Ser 97:183–192. doi:10.3354/meps097183

Bayne BL (1976) Marine mussels: their ecology and physiology. Cambridge University Press, Cambridge

Bougrier S, Geairon P, Deslous-Paoli JM, Bacher C, Jonquières G (1995) Allometric relationships and effects of temperature on clearance and oxygen consumption rates of *Crassostrea gigas* (Thunberg). Aquaculture 134:143–154. doi:10.1016/0044-8486(95)00036-2

Butman CA, Fréchette M, Geyer WR, Starczak VR (1994) Flume experiments on food supply to the blue mussel *Mytilus edulis* L. as a function of boundary-layer flow. Limnol Oceanogr 39:1755–1768

Ciutat A, Widdows J, Pope ND (2007) Effect of *Cerastoderma edule* density on near-bed hydrodynamics and stability of cohesive muddy sediments. J Exp Mar Biol Ecol 346:114–126. doi:10.1016/j.jembe.2007.03.005

Dame RF (1996) Ecology of marine bivalves: an ecosystem approach. CRC Press, Boca Raton

Dankers N, Meijboom A, de Jong M, Dijkman E, Cremer J, Fey F, Smaal A, Craeymeersch J, Brummelhuis E, Steenbergen J, Baars D (2006) De ontwikkeling van de Japanse Oester in Nederland. Wageningen IMARES, Report C040/06, Yerseke

Dolmer P (2000) Algal concentration profiles above mussel beds. J Sea Res 43:113–119. doi:10.1016/S1385-1101(00)00005-8

Drinkwaard AC (1999a) History of cupped oyster in european coastal waters. Aquac Eur 15:7–14 +41

Drinkwaard AC (1999b) Introductions and developments of oysters in the North Sea area: a review. Helgol Meersunters 52:301–308. doi:10.1007/BF02908904

Dupuy C, Vaquer A, Lam-Höai T, Rougier C, Mazouni N, Lautier J, Collos Y, Le Gall S (2000) Feeding rate of the oyster *Crassostrea gigas* in a natural planktonic community of the Mediterranean Thau Lagoon. Mar Ecol Prog Ser 205:171–184. doi:10.3354/meps205171

Ertman SC, Jumars PA (1988) Effects of bivalve siphonal currents on the settlement of inert particles and larvae. J Mar Res 46:797–813. doi:10.1357/002224088785113342

Famme P, Riisgård HU, Jørgensen CB (1986) On direct measurement of pumping rates in the mussel *Mytilus edulis*. Mar Biol (Berl) 92:323–327. doi:10.1007/BF00392672

Fernandes S, Sobral P, Van Duren L (2007) Clearance rates of *Cerastoderma edule* under increasing current velocity. Cont Shelf Res 27:1104–1115. doi:10.1016/j.csr.2006.08.010

Foster-Smith RL (1975) The effect of concentration of suspension on the filtration rates and pseudofaecal production for *Mytilus edulis* L., *Cerastoderma edule* (L.) and *Venerupis pullastra* (Montagu). J Exp Mar Biol Ecol 17:1–22. doi:10.1016/0022-0981(75)90075-1

Frank DM, Ward JE, Shumway SE, Holohan BA, Gray C (2008) Application of particle image velocimetry to the study of suspension feeding in marine invertebrates. Mar Freshw Behav Physiol 41:1–18. doi:10.1080/10236240801896207

Fréchette M, Butman CA, Geyer WR (1989) The importance of boundary-layer flows in supplying phytoplankton to the benthic suspension feeder, *Mytilus edulis* L. Limnol Oceanogr 34:19–36

Gerdes D (1983) The Pacific oyster *Crassostrea gigas.* Part I. Feeding behaviour of larvae and adults. Aquaculture 31:195–219. doi:10.1016/0044-8486(83)90313-7

Geurts van Kessel AJM, Kater BJ, Prins TC (2003) Veranderende draagkracht van de Oosterschelde voor kokkels. National Institute for Coastal and Marine Management (RIKZ) & Netherlands Institute for Fisheries Research (RIVO), Report RIKZ/2003.043/RIVO C062/03, Middelburg, the Netherlands

Gosling E (2003) Bivalve molluscs. Biology, ecology and culture. Blackwell, Oxford

Green S, Visser AW, Titelman J, Kiørboe T (2003) Escape responses of copepod nauplii in the flow field of the blue mussel, *Mytilus edulis*. Mar Biol (Berl) 142:727–733

Hawkins AJS, Fang JG, Pascoe PL, Zhang JH, Zhang XL, Zhu MY (2001) Modelling short-term responsive adjustments in particle clearance rate among bivalve suspension-feeders: separate unimodal effects of seston volume and composition in the scallop *Chlamys farreri*. J Exp Mar Biol Ecol 262:61–73

Helm MM, Bourne N, Lovatelli A (2004) Hatchery culture of bivalves—a practical manual. In: Lovatelli A (ed) FAO fisheries technical paper, Rome, p 177

Hinsch KD (1993) Particle image velocimetry. In: Sirohi RS (ed) Speckle metrology. Marcel Dekker, New York, pp 235–324

Jones HD, Richards OG, Southern TA (1992) Gill dimensions, water pumping rate and body size in the mussel *Mytilus edulis* L. J Exp Mar Biol Ecol 155:213–237. doi:10.1016/0022-0981(92)90064-H

Jonsson PR, Petersen JK, Karlsson Ö, Loo L-O, Nilsson S (2005) Particle depletion above experimental bivalve beds: in situ measurements and numerical modelling of bivalve filtration in the boundary layer. Limnol Oceanogr 50:1989–1998

Kamermans P (1993) Food limitation in cockles (*Cerastoderma edule* (L.)): influences of location on tidal flat and of nearby presence of mussel beds. Neth J Sea Res 31:71–81. doi:10.1016/0077-7579(93)90019-O

Kiørboe T, Visser AW (1999) Predator and prey perception in copepods due to hydromechanical signals. Mar Ecol Prog Ser 179:81–95. doi:10.3354/meps179081

Kiørboe T, Saiz E, Visser AW (1999) Hydrodynamic signal perception in the copepod *Acartia tonsa*. Mar Ecol Prog Ser 179:97–111. doi:10.3354/meps179097

Larsen PS, Riisgård HU (1997) Biomixing generated by benthic filter feeders: a diffusion model for near-bottom phytoplankton depletion. J Sea Res 37:81–90. doi:10.1016/S1385-1101(97)00009-9

Lassen J, Kortegård M, Riisgård HU, Friedrichs M, Graf G, Larsen PS (2006) Down-mixing of phytoplankton above filter-feeding mussels—interplay between water flow and biomixing. Mar Ecol Prog Ser 314:77–88. doi:10.3354/meps314077

Lehane C, Davenport J (2002) Ingestion of mesozooplankton by three species of bivalve; *Mytilus edulis, Cerastoderma edule* and *Aequipecten opercularis*. J Mar Biol Assoc U K 82:615–619. doi:10.1017/S0025315402005957

Maar M, Nielsen TG, Bolding K, Burchard H, Visser AW (2007) Grazing effects of blue mussel *Mytilus edulis* on the pelagic food web under different turbulence conditions. Mar Ecol Prog Ser 339:199–213. doi:10.3354/meps339199

Maas Geesteranus RA (1942) On the formation of banks by *Mytilus edulis* L. Arch Neerl Zool 6:283–326

Møhlenberg F, Riisgård HU (1978) Efficiency of particle retention in 13 species of suspension feeding bivalves. Ophelia 17:239–246

Møhlenberg F, Riisgård HU (1979) Filtration rate, using a new indirect technique, in thirteen species of suspension-feeding bivalves. Mar Biol (Berl) 54:143–147. doi:10.1007/BF00386593

Newell CR, Wildish DJ, MacDonald BA (2001) The effects of velocity and seston concentration on the exhalant siphon area, valve gape and filtration rate of the mussel *Mytilus edulis*. J Exp Mar Biol Ecol 262:91–111. doi:10.1016/S0022-0981(01)00285-4

Nikora V, Green MO, Thrush SF, Hume TM, Goring D (2002) Structure of the internal boundary layer over a patch of pinnid bivalves (*Atrina zelandica*) in an estuary. J Mar Res 60:121–150. doi:10.1357/002224002762341276

Norušis MJ (2008) SPSS 16.0 statistical procedures companion. Prentice Hall, Upper Saddle River. ISBN-13: 978-0-13-606139-7

O'Riordan CA, Monismith SG, Koseff JR (1995) The effect of bivalve excurrent jet dynamics on mass transfer in a benthic boundary layer. Limnol Oceanogr 40:330–344

Petersen JK, Bougrier S, Smaal AC, Garen P, Robert S, Larsen JEN, Brummelhuis EBM (2004) Intercalibration of mussel *Mytilus edulis* clearance rate measurements. Mar Ecol Prog Ser 267:187–194. doi:10.3354/meps267187

Porter ET, Cornwell JC, Sanford LP (2004) Effect of oysters *Crassostrea virginica* and bottom shear velocity on benthic-pelagic coupling and estuarine water quality. Mar Ecol Prog Ser 271:61–75. doi:10.3354/meps271061

Prins TC, Smaal AC, Pouwer AJ, Dankers N (1996) Filtration and resuspension of particulate matter and phytoplankton on an intertidal mussel bed in the Oosterschelde estuary (SW Netherlands). Mar Ecol Prog Ser 142:121–134. doi:10.3354/meps142121

Riisgård HU (1977) On measurements of the filtration rates of suspension feeding bivalves in a flow system. Ophelia 16:167–173

Riisgård HU (2001) On measurement of filtration rates in bivalves—the stony road to reliable data: review and interpretation. Mar Ecol Prog Ser 211:275–291. doi:10.3354/meps211275

Riisgård HU, Larsen PS (2000) Comparative ecophysiology of active zoobenthic filter feeding, essence of current knowledge. J Sea Res 44:169–193. doi:10.1016/S1385-1101(00)00054-X

Riisgård HU, Randløv A (1981) Energy budgets, growth and filtration rates in *Mytilus edulis* at different algal concentrations. Mar Biol (Berl) 61:227–234. doi:10.1007/BF00386664

Riisgård HU, Kittner C, Seerup DF (2003) Regulation of opening state and filtration rate in filter-feeding bivalves (*Cardium edule, Mytilus edulis, Mya arenaria*) in response to low algal concentrations. J Exp Mar Biol Ecol 284:105–127. doi:10.1016/S0022-0981(02)00496-3

Singarajah KV (1969) Escape reactions of zooplankton: the avoidance of a pursuing siphon tube. J Exp Mar Biol Ecol 3:171–178. doi:10.1016/0022-0981(69)90015-X

Singarajah KV (1975) Escape reactions of zooplankton: effects of light and turbulence. J Mar Biol Assoc U K 55:627–639

Smaal AC, Twisk F (1997) Filtration and absorption of *Phaecystis* cf. *globosa* by the mussel *Mytilus edulis* L. J Exp Mar Biol Ecol 209:33–46. doi:10.1016/S0022-0981(96)02695-0

Spedding GR, Rignot EJM (1993) Performance analysis and application of grid interpolation techniques for fluid flows. Exp Fluids 15:417–430. doi:10.1007/BF00191784

Stamhuis EJ (2006) Basics and principles of particle image velocimetry (PIV) for mapping biogenic and biologically relevant flows. Aquat Ecol 40:463–479. doi:10.1007/s10452-005-6567-z

Stamhuis EJ, Videler JJ, Duren LAV, Müller UK (2002) Applying digital particle image velocimetry to animal-generated flows: Traps, hurdles and cures in mapping steady and unsteady flows in Re regimes between 10–2 and 105. Exp Fluids 33:801–813

Tamburri MN, Zimmer RK, Zimmer CA (2007) Mechanisms reconciling gregarious larval settlement with adult cannibalism. Ecol Monogr 77:255–268. doi:10.1890/06-1074

Titelman J, Kiørboe T (2003) Predator avoidance by nauplii. Mar Ecol Prog Ser 247:137–149. doi:10.3354/meps247137

Tritton DJ (1988) Physical fluid dynamics. Oxford University Press, New York

Troost K, Kamermans P, Smaal AC, Wolff WJ (submitted) The effect of bivalve filter feeders on bivalve larval abundance in the Oosterschelde estuary (SW Netherlands) at different spatial scales. Submitted for publication in the Journal of Sea Research

Vahl O (1972) Porosity of the gill, oxygen consumption and pumping rate in *Cardium edule* (L.) (Bivalvia). Ophelia 10:109–118

Van Duren L, Herman PMJ, Sandee AJJ, Heip CHR (2006) Effects of mussel filtering activity on boundary layer structure. J Sea Res 55:3–14. doi:10.1016/j.seares.2005.08.001

Visser AW (2001) Hydromechanical signals in the plankton. Mar Ecol Prog Ser 222:1–24. doi:10.3354/meps222001

Walne PR (1972) The influence of current speed, body size and water temperature on the filtration rate of five species of bivalves. J Mar Biol Assoc U K 52:345–374

Widdows J, Navarro JM (2007) Influence of current speed on clearance rate, algal cell depletion in the water column and resuspension of biodeposits of cockles (*Cerastoderma edule*). J Exp Mar Biol Ecol 343:44–51. doi:10.1016/j.jembe.2006.11.011

Wildish D, Kristmanson D (1997) Benthic suspension feeders and flow. Cambridge University Press, Cambridge

Wiles PJ, Van Duren LA, Häse C, Larsen J, Simpson JH (2006) Stratification and mixing in the Limfjorden in relation to mussel culture. J Mar Syst 60:129–143. doi:10.1016/j.jmarsys.2005.09.009

Winter JE (1973) The filtration rate of *Mytilus edulis* and its dependence on algal concentration, measured by a continuous automatic recording apparatus. Mar Biol (Berl) 22:137–328. doi:10.1007/BF00391388

Wolff WJ, Reise K (2002) Oyster imports as a vector for the introduction of alien species into northern and western European coastal waters. In: Leppäkoski E, Gollasch S, Olenin S (eds) Invasive aquatic species of Europe. Distribution, impacts and management. Kluwer, Dordrecht, pp 193–205

Wong WH, Levinton JS (2004) Culture of the blue mussel *Mytilus edulis* (Linnaeus, 1758) fed both phytoplankton and zooplankton: a microcosm experiment. Aquacult Res 35:965–969. doi:10.1111/j.1365-2109.2004.01107.x

Wong WH, Levinton JS (2006) The trophic linkage between zooplankton and benthic suspension feeders: direct evidence from analyses of bivalve faecal pellets. Mar Biol (Berl) 148:799–805. doi:10.1007/s00227-005-0096-0

Wright LD, Friedrichs CT, Hepworth DA (1997) Effects of benthic biology on bottom boundary layer processes, dry Tortugas Bank, Florida Keys. Geo-Mar Lett 17:291–298. doi:10.1007/s003670050040